Cancer Cell
Article

Suppression of miRNA-708 by Polycomb Group Promotes Metastases by Calcium-Induced Cell Migration

Seongho Ryu,[1,2] Kevin McDonnell,[1,2,6] Hyejin Choi,[1,2] Dingcheng Gao,[1,2] Mary Hahn,[1,2] Natasha Joshi,[1,2] Sun-Mi Park,[1] Raul Catena,[1,2] Yoonkyung Do,[5] Jacqueline Brazin,[4] Linda T. Vahdat,[3] Randi B. Silver,[4] and Vivek Mittal[1,2,*]
[1]Department of Cardiothoracic Surgery
[2]Department of Cell and Developmental Biology
[3]Department of Medicine
[4]Department of Physiology and Biophysics
Weill Cornell Medical College of Cornell University, 1300 York Avenue, 525 East 68th Street, New York, NY 10065, USA
[5]Ulsan National Institute of Science and Technology, School of Nano-Bioscience and Chemical Engineering, Ulsan 689-798, South Korea
[6]Present address: Michigan State University, East Lansing, MI 48824, USA
*Correspondence: vim2010@med.cornell.edu
http://dx.doi.org/10.1016/j.ccr.2012.11.019

SUMMARY

The progression of cancer to metastatic disease is a major cause of death. We identified miR-708 being transcriptionally repressed by polycomb repressor complex 2-induced H3K27 trimethylation in metastatic breast cancer. miR-708 targets the endoplasmic reticulum protein neuronatin to decrease intracellular calcium level, resulting in reduction of activation of ERK and FAK, decreased cell migration, and impaired metastases. Ectopic expression of neuronatin refractory to suppression by miR-708 rescued cell migration and metastasis defects. In patients with breast cancer, miR-708 expression was decreased in lymph node and distal metastases, suggesting a metastasis-suppressive role. Our findings uncover a mechanistic role for miR-708 in metastasis and provide a rationale for developing miR-708 as a therapeutic agent against metastatic breast cancer.

INTRODUCTION

Malignant primary tumor cells colonize distal organs to form metastases resulting in more than 90% of cancer-related deaths (Gupta and Massagué, 2006; Steeg, 2006). Many studies have investigated cancer cell intrinsic mechanisms and the extrinsic microenvironmental factors that enhance the metastatic potential of primary tumor cells (Fidler, 2003; Gupta and Massagué, 2006; Joyce and Pollard, 2009). The metastatic cascade comprises a series of steps to accomplish invasion, migration, dissemination, and colonization of target organs to generate lethal metastases. However, our understanding of the regulators that mediate the metastatic cascade has remained incomplete.

MicroRNAs (miRNAs) are small, noncoding RNAs (18–23 nucleotides in size) that regulate gene expression by sequence-specific binding to messenger RNA (mRNA) and trigger translation repression or RNA degradation (Bartel, 2004). miRNAs play important roles in various biological processes, including cell growth, differentiation, and development (Alvarez-Garcia and Miska, 2005; Inui et al., 2010). Abnormal miRNA expression has been reported in various diseases including cancer (Calin and Croce, 2006; Lu et al., 2005; Ozen et al., 2008; Volinia et al., 2006). More than 50% of miRNA-encoding loci reside in chromosomal regions altered during tumorigenesis (Calin et al., 2004), and expression profiling reveals characteristic miRNA signatures for many tumor types, including breast neoplasia, that predict disease status and clinical outcome (Calin and Croce, 2006). In addition, miRNAs have been identified that function as oncogenes or tumor suppressor genes (Magalhaes et al., 2002; Ventura et al., 2008),

Significance

Patients with triple-negative breast cancer (TNBC) have the worst outcome among patients with breast cancer due to high propensity for recurrence and metastatic spread. Furthermore, to our knowledge, there is no approved targeted therapy for treatment of TNBC. Here, we show that the expression of miR-708 is reduced during metastatic progression of breast cancer. We demonstrate that polycomb repressor complex 2-mediated suppression of miR-708 increases expression of neuronatin, which elevates intracellular Ca^{2+} levels to promote cell migration and metastasis formation. Together, these findings support the notion that miR-708 is a potential therapeutic against metastatic breast cancer.

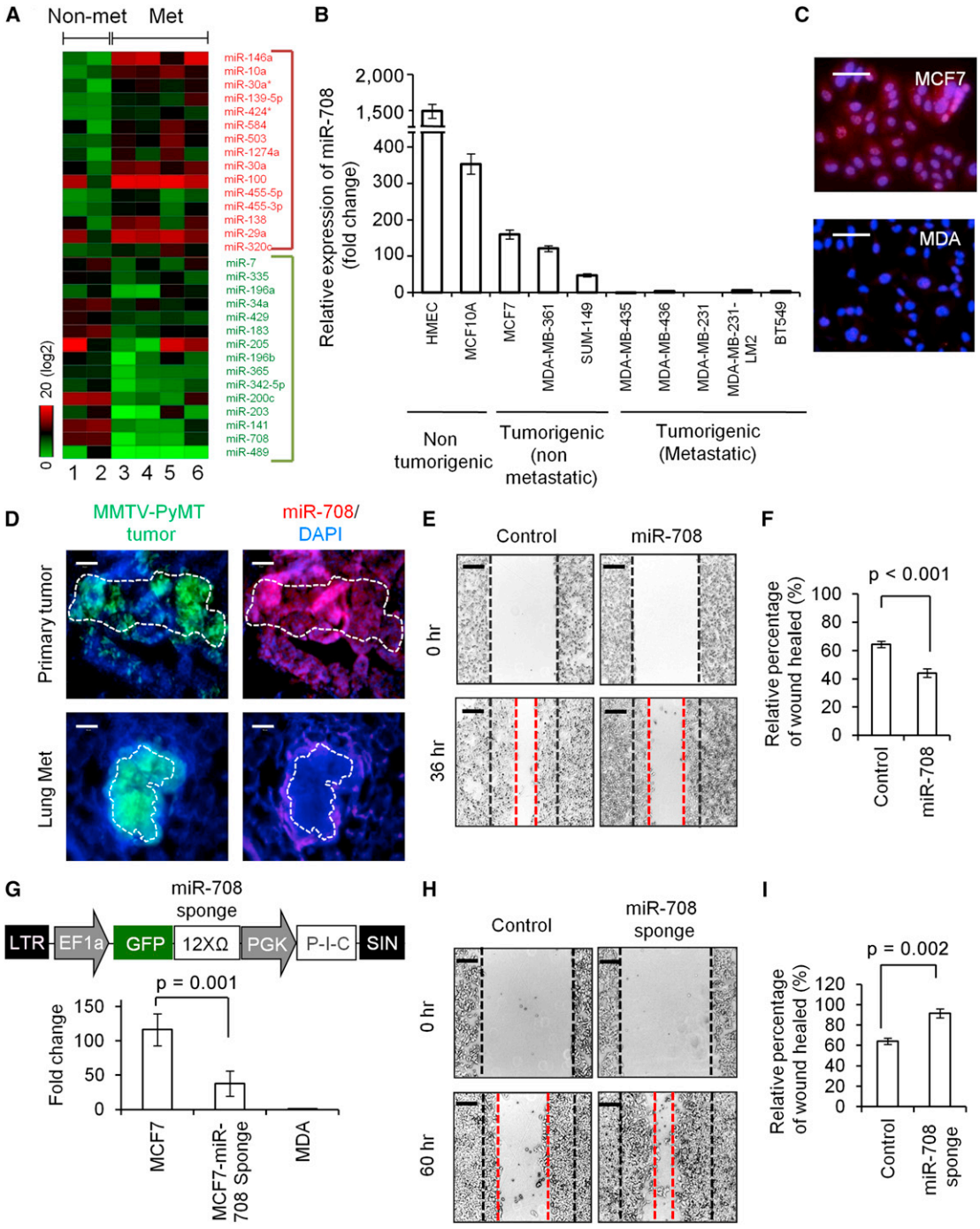

Figure 1. miR-708 Is Downregulated in Metastatic Cancer Cells and Affects Cell Migration

(A) Heatmap obtained from high-throughput miR-seq profiling of nontumorigenic breast epithelial cells (MCF-10A, lane 1) and nonmetastatic (Non-met) (MCF7, lane 2) and metastatic breast cancer cell lines (MDA, lanes 3 and 4; LM2, lanes 5 and 6). Each row represents a miRNA that is differentially regulated (2-fold or more in sequence-read frequencies), and each column represents the average of two biological replicates. The relatively high expression is indicated in red, whereas the relatively low expression is in green.

(B) Quantitative RT-PCR analysis of miR-708 in a panel of nontumorigenic and tumorigenic (nonmetastatic and metastatic) breast cells. miR-708 expression analysis was performed in triplicate and normalized to the internal control, RNU48. y Axis depicts fold change in miR-708. Data represent mean ± SD.

(C) Microscopy images showing miR-708 in situ hybridization (red) in nonmetastatic MCF-7 cells (MCF7, top) and metastatic MDA (bottom) breast cancer cells. Scale bars, 50 μm.

(D) In situ hybridization of miR-708 (red) in GFP$^+$ primary breast tumors (Primary tumor) and lung metastases (Lung Met) in *MMTV-PyMT;WAP-Cre;CAG-CAT-EGFP* mice. Dotted line indicates primary tumor (green) in mammary gland and metastatic lesion (green) in the lung. DAPI was used to label the nuclei of all cells. Scale bars, 50 μm.

(legend continued on next page)

and some act at late stages of tumor progression (Ma et al., 2007; Tavazoie et al., 2008; Ventura et al., 2008; Huang et al., 2008; Asangani et al., 2008; Zhu et al., 2008; Lujambio et al., 2008). Recent studies have identified miRNAs that contribute to the pathophysiology of breast cancer via mechanisms enabling invasion and metastasis (Huang et al., 2008; Iorio et al., 2005; Ma et al., 2007; Valastyan et al., 2009), epithelial-to-mesenchymal transition (Bracken et al., 2009; Gregory et al., 2008), and maintenance of breast stem cells (Shimono et al., 2009).

Despite these studies, the role of miRNAs in specifically affecting the later steps in the metastatic cascade without confounding influences on primary tumor development has remained unclear (Ma et al., 2007; Valastyan et al., 2009; Valastyan and Weinberg, 2009). From a clinical translation perspective, whereas blocking primary tumor invasion and dissemination is considered an effective approach in blocking metastasis, an important question is how best to treat patients whose tumor has already metastasized. Thus, approaches are required to block widespread tumor dissemination and outgrowth in secondary organs for effective treatment of metastatic breast cancer. Considering the emerging roles of miRNAs in cancer biology, we set out to identify miRNAs that impact metastasis without affecting primary tumor growth and addressed its underlying molecular mechanisms and therapeutic potential against metastatic breast cancer.

RESULTS AND DISCUSSION

Identification of Differentially Regulated miRNAs in Metastasis

To identify miRNAs that regulate the metastatic cascade without affecting primary tumor growth, we performed next-generation miRNA sequencing (miR-seq) on human breast epithelial cell lines with different tumorigenic and metastatic potentials (Kang et al., 2009; Minn et al., 2005) (Table S1 available online). Total RNA was processed to generate libraries for miR-seq, and sequence reads obtained from each breast cancer cell line in duplicate were used for identifying miRNAs as described (Ryu et al., 2011). Alignment of sequence reads to known miRNA sequences in the miRNA database (miRBase v.16) revealed ~80% of reads that matched known human miRNAs (Table S2). Hierarchical clustering analysis revealed groups of differentially regulated miRNAs (Figure 1A), and miRNAs that were up- and downregulated in metastatic tumor cells were identified (Tables S3 and S4). As expected, we also identified previously discovered metastatic miRNAs including miR-200 family, miR-10, and miR-196 (Valastyan and Weinberg, 2009), validating our miRNA-profiling approach.

miR-708 Is Downregulated in Metastatic Tumor Cells Both In Vitro and In Vivo

From the list of differentially regulated miRNAs, we focused on miR-708 because it was one of the most downregulated miRNAs in metastatic tumor cells. Although miR-708 is highly conserved across species (Figure S1A), its role in tumor metastasis is unclear. Analysis of miR-708 expression levels in a panel of human breast cancer cell lines showed that miR-708 was markedly suppressed in metastatic cells compared with tumorigenic but nonmetastatic cells (Figure 1B). In agreement with RT-PCR analysis, in situ hybridization with a miR-708-locked nucleic acid (LNA) probe showed abundant miR-708 expression in nonmetastatic MCF7 cells, compared with metastatic MDA-MB-231 (MDA) cells (Figure 1C). Further analysis showed lower levels of miR-708 in basal subtype breast cancer cell lines compared to luminal subtype (Figure S1B). Consistent with cell lines, basal/triple-negative breast cancer (TNBC) subtype of human breast cancers had lower levels of miR-708 compared to the luminal subtype (Figure S1C). To evaluate miR-708 expression in spontaneous metastatic mammary tumors, we used the MMTV-PyMT mouse model, which develops primary breast tumors (6–7 weeks of age) that progress and give rise to metastases in the lungs (12–16 weeks of age) (Guy et al., 1992; Gao et al., 2008; Nolan et al., 2007). To reliably detect tumor cells at both the primary sites and in the metastatic organs, we used the *MMTV-PyMT; WAP-Cre;CAG-CAT-EGFP* mice that express GFP in mammary tumor cells (Ahmed et al., 2002), thus enabling the analysis of GFP-tagged primary tumors and matched pulmonary metastases in immunocompetent mice. In situ hybridization with the miR-708 LNA probe showed miR-708 expression in GFP^+ primary breast tumors, as expected. However, the GFP^+ pulmonary metastases were devoid of miR-708 expression (Figures 1D and S1D), an observation further confirmed by RT-PCR analysis of several excised primary tumors and matched metastases (Figure S1E). As a control, expression of ubiquitously expressing U6 snRNA remained unchanged (Figure S1E).

Having demonstrated suppression of miR-708 expression in metastatic cancer cells, we sought to evaluate the antimetastatic role of miR-708. A lentiviral delivery system (Ryu et al., 2011) was

(E) Representative images depicting a cell migration assay performed with 1×10^6 MDA control (Control) and MDA expressing miR-708 (miR-708) cells. Cells were plated into 6-well dishes and allowed to grow for 12 hr, after which a scratch was created, and cells were imaged immediately (0 hr) and at 36 hr. Scale bars, 200 μm.

(F) Cell migration was quantified as percentage of wound-healed area. Data represent mean ± SD of nine randomly selected areas from three independent experiments.

(G) Upper panel is a schematic of a lentiviral vector expressing miRNA "sponge." EF1α, elongation factor 1 α promoter; PGK, phosphoglycerate kinase gene promoter; P-I-C, puromycin-IRES-CFP; LTR, long-terminal repeat and sponge (12XΩ); 12 miR-708 binding sites. Lower panel is a quantitative RT-PCR showing fold change in miR-708 expression levels in MCF7 cells stably expressing the miR-708 sponge compared with MCF7 (MCF7-miR-708 sponge) and MDA controls (MDA). Data represent mean ± SD.

(H) Representative images depicting a cell migration assay performed with 1×10^6 MCF7 control (Control) and MCF7 "sponge" (miR-708 sponge) cells. Cells were plated into 6-well dishes and allowed to grow for 12 hr, after which a scratch was created, and cells were imaged immediately (0 hr) and 60 hr. Scale bars, 200 μm.

(I) Cell migration was quantitated as percentage of wound-healed area from MCF7 control (Control) and MCF7 "sponge" (miR-708 sponge) cells. Data represent mean ± SD of nine randomly selected areas from three independent experiments.

See also Tables S1–S4 and Figure S1.

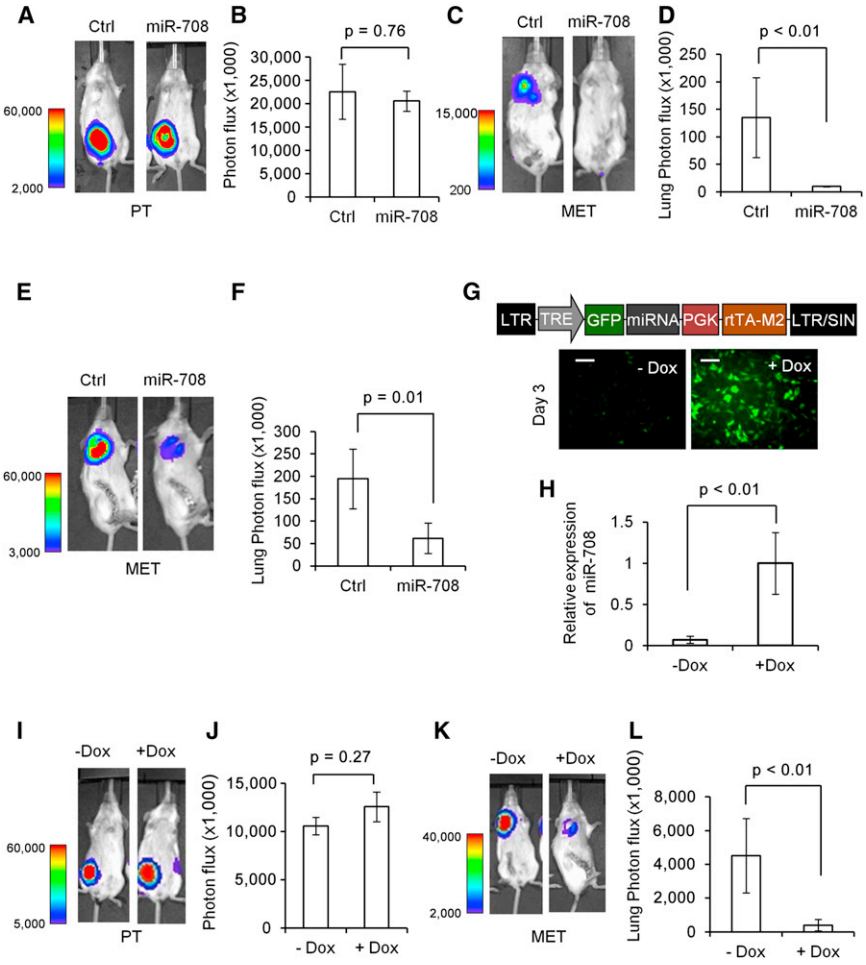

Figure 2. miR-708 Expression Attenuates Metastasis In Vivo

(A) Representative bioluminescence (BLI) images of animals showing primary tumors (PT) at day 60 derived from orthotopic injections into the mammary fat pad of MDA vector control (Ctrl) and MDA expressing miR-708 (miR-708) cells. The color scale bar depicts the photon flux (photons per second) emitted from these mice.

(B) Quantitation of primary tumors as assessed by BLI measurements (day 60, n = 10 per group). Data represent mean ± SD.

(C) Representative BLI of animals from (A) showing lung metastases (MET) at day 74. In this case, primary tumors were resected at day 60. The color scale bar depicts the photon flux (photons per second) emitted from these mice.

(D) Quantitation of pulmonary metastases as assessed by BLI measurements (day 74, n = 10 per group). Data represent mean ± SD.

(E) Representative BLI of animals showing lung metastases derived from orthotopic injections into the mammary fat pad of LM2 vector control (Ctrl) and MDA-MB-231-LM2-miR-708 (miR-708) cells at day 67. Primary tumors were resected at day 60. The color scale bar depicts the photon flux (photons per second) emitted from these mice.

(F) Quantitation of pulmonary metastases as assessed by BLI measurements (day 67, n = 10 per group). Data represent mean ± SD.

(G) Schematic of a lentiviral vector used for inducible expression and representative images of miR-708 following doxycycline (Dox) administration by food (200 mg/kg). Scale bars, 50 μm.

(H) Quantitative RT-PCR showing miR-708 expression levels in the presence of Dox (+Dox) or absence of Dox (−Dox). Data represent mean ± SD.

(I) Representative BLI of animals with primary tumors generated following orthotopic injections of MDA-MB-231-miR-708 in the mammary glands of SCID mice in the presence of Dox (+Dox) or absence of Dox (−Dox) at day 60.

(J) Quantitation of primary tumors as assessed by BLI measurements (day 60, n = 10 per group). Data represent mean ± SD.

(K) Representative BLI of animals showing lung metastases from (I) in the presence of Dox (+Dox) or absence of Dox (−Dox) (day 74). The primary tumors were resected at day 60.

(L) Quantitation of pulmonary metastases assessed by BLI measurements (day 67, n = 10 per group). Data represent mean ± SD.

See also Figure S2.

used to stably express miR-708 in metastatic human breast tumor cell lines MDA and MDA-MB-231-LM2 (LM2) (Figure S1F). MDA cells stably expressing miR-708 exhibited suppressed migration rates compared with controls (Figures 1E and 1F) but no significant change in cell proliferation (Figure S1G). Consistent with observations in breast cancer, ectopic expression of miR-708 also suppressed migration of metastatic prostate cancer cell PC3 (Figure S1H). Having observed that overexpression of miR-708 in metastatic breast cancer cells inhibited migration, we asked whether inhibiting miR-708 in nonmetastatic breast cancer cells might stimulate migration. To address this, we constructed a lentiviral vector expressing a miRNA-708 "sponge," a strategy that has previously been used for miRNA blockade (Ebert et al., 2007; Valastyan et al., 2009), to suppress miR-708 expression (Figure 1G). As expected, the "miR-708 sponge" inhibited miR-708 expression by >2-fold (Figure 1G), and miR-708 loss of function enhanced migration rates of MCF7 cells (Figures 1H and 1I). These results demonstrate that metastatic breast cancer cells exhibit lower levels of miR-708, and ectopic expression of miR-708 attenuates cell migration. In contrast, nonmetastatic breast cancer cells exhibit higher levels of miR-708, and suppression of miR-708 enhances cell migration.

miR-708 Expression Impairs the Formation of Metastases

To explore whether enhanced migration conferred a metastatic advantage to breast cancer cells in vivo, we injected MDA cells stably expressing miR-708 and a luciferase reporter transgene orthotopically into the mammary fat pad of mice. Bioluminescence imaging (BLI) showed no significant difference in the primary tumor growth but a significant reduction in lung metastases as a result of miR-708 expression (Figures 2A–2D). We confirmed the antimetastatic role of miR-708 in LM2. Consistent with previous observations, primary tumor growth in LM2 overexpressing miR-708 remained unperturbed; however, there was a pronounced reduction in lung metastases (Figures 2E,

2F, S2A, and S2B). To exclude the remote possibility that constitutive expression of miR-708 during the establishment of stable breast cancer cells could have inadvertently conferred an antimetastatic phenotype, a doxycycline-based conditional expression of miR-708 was used (Gao et al., 2008; Stegmeier et al., 2005). This approach allowed us to generate acute miR-708 expression only after the cells were administered in vivo. miR-708 was cloned into a doxycycline-inducible vector, and the specific and tight regulation of miR-708 expression by the inducible system was assessed in vitro (Figures 2G and 2H). Administration of these cells into the mammary fat pad of SCID mice followed by doxycycline-mediated induction of miR-708 did not affect primary tumor growth (Figures 2I and 2J) but attenuated metastases (Figures 2K and 2L), consistent with results using the constitutive system. Although miR-708 loss of function enhanced migration rates in the MCF7 model, it was not sufficient to promote metastasis in vivo (data not shown), suggesting that the MCF7 cells may need additional prometastatic properties to accomplish successful metastasis. Taken together, these results demonstrate that expression of miR-708 in metastatic breast cancer cells attenuates metastasis formation in vivo but did not impact primary tumor growth, which provided an opportunity to determine its role in the later steps of metastatic progression.

miR-708 Suppresses Expression of Neuronatin, a Regulator of Intracellular Calcium

To identify downstream effectors of miR-708, we used mRNA target-predicting algorithms (TargetScan, miRanda, and TargetRank) based on the presence of binding sites in the 3′ UTR. Of the seven genes that overlapped among these algorithms (Figure 3A), we selected four genes (*GON4L*, *HOXB3*, *NNAT*, and *CNTFR*) that were associated with metastasis-related functions such as cell proliferation, apoptosis, cell cycle, migration, adhesion, invasion, and cell differentiation (Figures S3A and S3B). We also selected six genes (*SSH2*, *EPDR1*, *SSRP1*, *HNRNPK*, *YWAHZ*, and *USP9X*) with prometastatic function that were predicted by more than one algorithm (Figure S3A) and three additional genes (*CD44*, *ENAH*, and *NTRK2*) that had multiple binding sites predicted by an independent algorithm developed in-house.

To establish a direct relationship between miR-708 and predicted target genes, we cloned the 3′ UTR of key target genes into a dual-luciferase UTR vector (Figure 3B). Notably, 3′ UTR of *NNAT* (which encodes neuronatin), *GON4L*, *NTRK2*, and *CD44* appeared to be repressed by miR-708 (Figure 3B). However, at the protein level, of the genes tested, expression of neuronatin protein was significantly decreased by miR-708 (Figure 3C), consistent with RT-PCR analysis (Figure S3C). We also evaluated *AKT2*, which was recently reported to be a target of miR-708 in primary prostate cancer (Saini et al., 2012), but did not find it to be suppressed by miR-708 in breast cancer (data not shown). Consistent with the constitutive expression system, doxycycline-mediated acute and conditional expression of miR-708 also suppressed neuronatin levels (Figure S3D). As would be expected, there existed an inverse correlation between miR-708 and *NNAT* levels in MCF7 and MDA cells (Figures 1B and S3C).

Evaluation of the 3′ UTR sequence of *NNAT* revealed one binding site with perfect matches both in the seed and flanking sequences for miR-708 (Figures 3D and S3E). Notably, both miR-708 and the binding site in the *NNAT* are highly conserved across species (Figure S3F). We next generated mutations in the binding site to abrogate miR-708-*NNAT* 3′ UTR interaction (Figure 3D). As expected, whereas a reporter with an intact *NNAT* 3′ UTR was effectively suppressed by miR-708, that with *NNAT* 3′ UTR carrying a mutated binding site was refractory to suppression by miR-708 (Figure 3E). To determine if *NNAT* with a 3′ mutant UTR (*NNAT*-mut) was also refractory to miR-708-mediated suppression, we expressed a cDNA that harbored a mutation in the 3′ UTR containing the miR-708 binding sites. This mutant UTR abolished miR-708-mediated suppression of the *NNAT* (Figure 3F). Having established that miR-708 regulates *NNAT* expression, we next determined if there was an inverse correlation between miR-708 and *NNAT* levels in the breast cancer cell lines examined in Figure 1. Notably, *NNAT* levels inversely correlated with miR-708 expression (Figure 3G). Taken together, these results indicate that miR-708 directly regulates *NNAT* expression through the perfect binding site in the 3′ UTR.

miR-708-Mediated Suppression of Neuronatin Impacts the Release of Store-Operated Ca^{2+}

Neuronatin is a membrane protein in the ER (Joseph et al., 1994) that resembles phospholamban, an inhibitor of sarcoplasmic reticulum Ca^{2+}-ATPase (SERCA). Neuronatin-mediated regulation of intracellular Ca^{2+} has been implicated in neural induction in embryonic stem cells (Lin et al., 2010) and in adipogenesis (Suh et al., 2005). Notably, Ca^{2+} is a critical regulator of cell migration (Pettit and Fay, 1998; Yang et al., 2009). We therefore hypothesized that miR-708-mediated targeting of *NNAT* may lead to impaired regulation of intracellular Ca^{2+}, which could explain the inhibitory effect on the migratory phenotype of metastatic tumor cells observed earlier (Figure 1E). To test this hypothesis, we monitored the intracellular Ca^{2+} levels in MDA and MDA expressing miR-708 (MDA-miR-708) cells in the absence and presence of exogenous ATP. ATP binds ATP receptors on the cell surface, resulting in the cleavage of PIP2 into IP3 and DAG. IP3 binds IP3 receptors on the ER membrane and releases ionized calcium from the ER (Vandewalle et al., 1994; Berridge et al., 2003; Swanson et al., 1998). Thus, ATP-stimulated calcium release from ER was used to evaluate the consequence of *NNAT* suppression by miR-708. As expected, MDA cells responded to ATP by exhibiting a rapid increase of Ca^{2+}, followed by a regulatory phase back to basal levels (Figure 4A). In contrast, MDA-miR-708 cells exhibited a similar Ca^{2+} transient but attenuated regulation of intracellular Ca^{2+}, indicating that *NNAT* knockdown by miR-708 may be responsible for the aberrant Ca^{2+} reuptake mechanism to the ER (Figure 4A). To directly demonstrate that suppression of *NNAT* by miR-708 was responsible for the decreased Ca^{2+} influx, we performed a rescue experiment by expressing *NNAT* cDNA with a 3′ mutant UTR in MDA-miR-708 (MDA-miR-708-*NNAT*-mut) cells. There were no differences in the basal intracellular Ca^{2+} levels or peak response to ATP among the MDA control, MDA-miR-708, and MDA-miR-708-*NNAT*-mut cells (Figure 4B). Strikingly, expression of the *NNAT*-mut rescued the defects in intracellular Ca^{2+} regulation in miR-708-expressing MDA cells (Figure 4C), as well as the migration phenotype (Figure 4D). Notably, expression

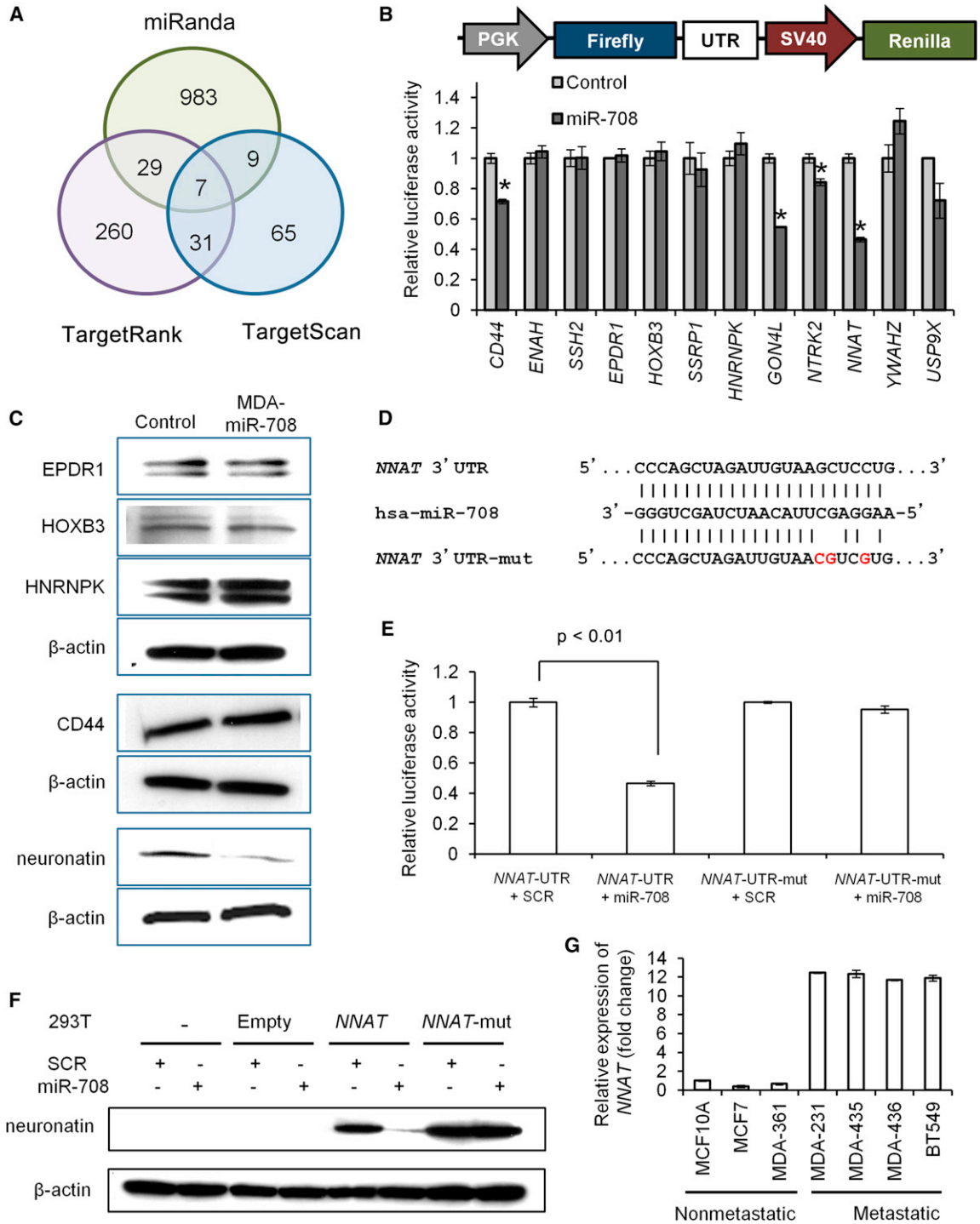

Figure 3. miR-708 Regulates Expression of Neuronatin

(A) Venn diagrams showing the number of genes identified as potential targets of miR-708 as predicted by three algorithms: TargetScan, miRanda, and TargetRank.

(B) A schematic of a dual-luciferase vector used for cloning 3′ UTR of candidate genes. Dual-luciferase assays showing that repression of candidate genes by miR-708 was measured as ratios of Renilla and Firefly luciferase activity in 293T cells. Data represent mean ± SD. *p < 0.01.

(C) Western blot analysis of endogenous candidate proteins in MDA (Control) and MDA-MB-231-miR-708 (MDA-miR-708) cells. β-Actin serves as an internal control.

(D) Sequences of miR-708 and the potential miR-708 binding site at the 3′ UTR of *NNAT*. Also shown are nucleotides mutated in *NNAT*-3′ UTR mutant.

(E) Dual-luciferase assays showing repression of wild-type UTR (*NNAT*-UTR) or mutant UTR (*NNAT*-UTR-mut) following transfection of synthetic miR-708 or scrambled (SCR) miRNA. Data represent mean ± SD.

(legend continued on next page)

of *NNAT*-mut alone in control MDA cells did not impact migration rates (Figures S4A–S4C). To directly demonstrate that the regulation of Ca^{2+} is the main reason for miR-708-*NNAT*-mediated migration phenotype, we used BAPTA-AM, an intracellular calcium chelator (Hoth and Penner, 1992). As expected, BAPTA-AM showed a dramatic impairment in MDA cell migration (Figures 4E, S4D, and S4E), whereas migration in MDA-miR708 cells remained less affected. More importantly, expression of *NNAT*-mut in MDA-miR-708 cells rescued the BAPTA-AM-induced cell migration defects. To exclude the possibility that the migration effects were not confined to the MDA cell line alone, we used another metastatic cell line, MDA-MB-436. Consistent with previous data, MDA-MB-436 cells expressing miR-708 also showed increased migration that remained less affected by BAPTA-AM (Figure S4F) and decreased levels of *NNAT* (Figure S4G). These results suggest that suppression of miR-708 in metastatic tumor cells is necessary for *NNAT* to maintain adequate levels of intracellular Ca^{2+} stores required for the migratory phenotype. Furthermore, the demonstration that miR-708 regulates *NNAT* expression provides an insight into Ca^{2+} regulation in metastatic tumor cells.

miR-708-Induced Aberrant Ca^{2+} Regulation Impacts Focal Adhesion Kinase

To further elucidate the mechanisms by which the miR-708-*NNAT*-Ca^{2+} axis regulates cell migration, we evaluated downstream signaling pathways. ATP-induced transient elevation of intracellular Ca^{2+} has been shown to trigger key components of numerous signaling pathways, including protein kinases such as the calmodulin-dependent kinases (CaMKs) and the extracellular signal-regulated kinases (ERKs) (Swanson et al., 1998). Following Ca^{2+} release by ATP, MDA cells showed a rapid and transient increase in phospho (p)-p44/ERK1 and p42/ERK2 over basal levels as compared with MDA-miR-708 cells (Figures 4F and S4H), suggesting that aberrant intracellular Ca^{2+} regulation in MDA-miR-708 cells may be responsible for reduced levels of activated ERK. Importantly, expression of mutant *NNAT* rescued p-ERK levels in MDA-miR-708 cells (Figures 4F and S4H). ERK has been implicated in the migration of numerous cell types by virtue of its ability to phosphorylate several protein kinases, including focal adhesion kinase (FAK) (Huang et al., 2004). Indeed, fibroblasts derived from *Fak* knockout mice show diminished migration ability (Ilić et al., 1995; Zhao and Guan, 2009). In fact, elevated level of basal p-FAK (S910) was observed in MDA compared to MDA-miR-708 cells (Figures 4F and S4I). Notably, following ATP-mediated Ca^{2+} release, p-FAK levels increased in MDA and not in MDA-miR-708 cells (Figures 4F and S4I). Again, as expected, expression of *NNAT* 3′ mutant UTR restored both the basal and ATP-induced p-FAK in MDA-miR-708 cells (Figures 4F and S4I). These data are consistent with previous reports showing that FAK phosphorylation at S910 (Hunger-Glaser et al., 2004) is associated with increased cell migration and metastasis (Zheng et al., 2009) and suggest that alleviated FAK activation may explain the attenuated migration attributes of miR-708-expressing cells. We next evaluated focal adhesions at the cellular level by immunostaining for vinculin, a well-known focal adhesion molecule, and p-FAK (S910). Strikingly, p-FAK colocalized well with vinculin$^+$ focal adhesions in MDA and MDA-miR-708-*NNAT* 3′ mutant UTR cells, whereas the focal adhesions in MDA-miR-708 cells remained devoid of p-FAK (Figure 4G). Furthermore, MDA-miR-708 cells exhibited thick bands of cortical actin rings around the cell's periphery (Figure S4J), a phenotype previously associated with migration defects in FAK null cells (Sieg et al., 1999).

Taken together, these results suggest that miR-708-induced aberrant Ca^{2+} levels are responsible for impacting ERK and FAK activation. Importantly, expressing *NNAT* with a mutant 3′ UTR that is refractory to miR-708 suppression in MCF7 cells rescued aberrant Ca^{2+} levels and promoted cell migration (Figure S4K). These data are also in agreement with a previous study showing that enhanced efflux of store-operated Ca^{2+} into the cytoplasm is critical for serum-induced breast cancer cell migration via induction of FAK (Yang et al., 2009).

PRC2 Is Involved in the Suppression of miR-708 in Metastatic Cells

In a previous study, chromatin immunoprecipitation and deep-sequencing (ChIP-seq) analysis of embryonic stem cells unraveled several miRNAs, including miR-708, regulated by the PcG repressor complex subunit SUZ12 (Marson et al., 2008). Consistent with this observation, genome-wide profiling of chromatin signatures in colorectal cancer revealed that miRNAs were also epigenetically regulated (Suzuki et al., 2011). These observations suggested that the PcG group of transcriptional repressors might suppress miR-708 in breast cancer metastasis. Two distinct PcG complexes, polycomb repressor complex 1 (PRC1) and PRC2, are critical to maintaining a repressed gene state (Schwartz and Pirrotta, 2007; Margueron et al., 2009; Simon and Kingston, 2009), and PRC2, which includes SUZ12 and the catalytic subunit EZH2, is responsible for di- and trimethylation of lysine 27 on histone H3 resulting in gene repression (Boyer et al., 2006; Cao et al., 2002; Koyanagi et al., 2005) (Cao and Zhang, 2004).

Western blot analysis of breast cancer cells showed upregulation of SUZ12 (approximately 7.5-fold) in metastatic MDA cells compared with controls (Figure 5A), consistent with observations in metastatic prostate and breast cancer (Bracken et al., 2009; Kleer et al., 2003; Sellers and Loda, 2002). To determine whether the miR-708 promoter associates with the PcG complex, we performed ChIP experiments for SUZ12 using cross-linked chromatin from nonmetastatic and metastatic breast cancer cells. The enriched DNA from the immunoprecipitates (IPs) was quantified by RT-PCR using primers spanning the miR-708 upstream regions (Figure 5B). Enrichment of SUZ12 was found to be associated with the miR-708 upstream region in metastatic MDA and LM2 cells compared with nonmetastatic

(F) Western blot analysis showing neuronatin levels expressed from *NNAT* cDNA with a wild-type UTR (*NNAT*) or mutant UTR (*NNAT*-mut) in the presence of synthetic miR-708 or scrambled (SCR) miRNA. β-Actin serves as an internal control.
(G) Quantitative RT-PCR showing *NNAT* expression in a panel of nonmetastatic and metastatic breast cancer cells. Data represent mean ± SD.
See also Figure S3.

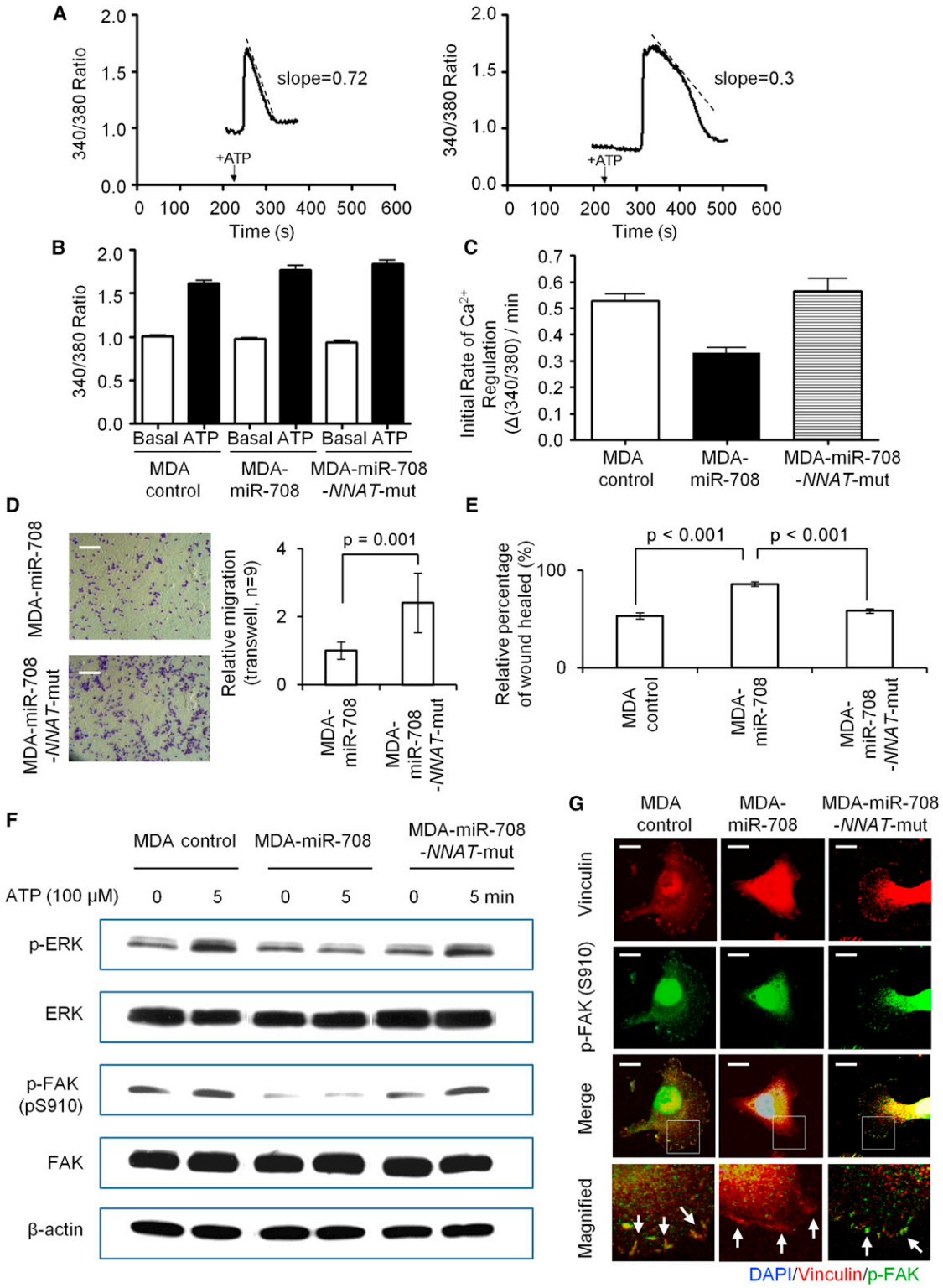

Figure 4. miR-708-Mediated Suppression of Neuronatin Results in Aberrant Ca^{2+} Regulation and Inactivation of ERK and FAK

(A) Representative calcium traces of MDA control (left panel) and MDA-MB-231-miR-708 cells (right panel) stimulated with ATP. The dotted lines represent the initial rate of calcium regulation back to baseline.

(B) Peak calcium responses due to ATP stimulation (MDA control, MDA-miR-708, MDA-miR-708-*NNAT*-mut, respectively; 1.61 ± 0.04, 1.77 ± 0.06, 1.84 ± 0.05). For ratios pre-ATP stimulation (basal), values are 1.00 ± 0.01, 0.97 ± 0.01, and 0.93 ± 0.02, respectively (n = 115, 107, and 72 cells, respectively). Transfection efficiency in MDA-miR-708-*NNAT*-mut cells was ~30%. Data are represented as mean ± SEM.

(legend continued on next page)

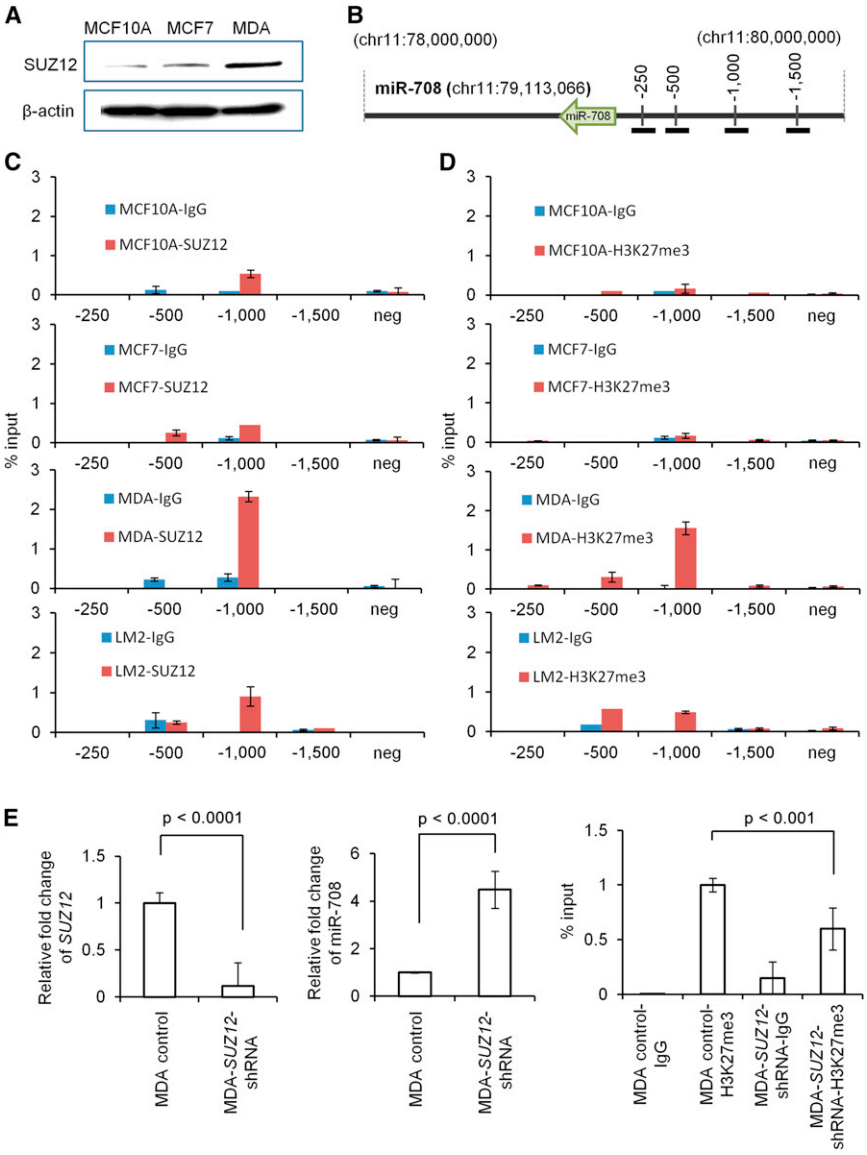

Figure 5. PRC2 Suppresses miR-708 Expression in Metastatic Tumor Cells

(A) Western blot showing SUZ12 levels in nontumorigenic (MCF10A), nonmetastatic (MCF7), and metastatic (MDA) breast cancer cells. β-Actin serves as an internal control. A 7.5-fold change was observed in MDA compared to MCF7.

(B) Schematic showing genomic location of miR-708. The upstream regions used for ChIP-PCR are indicated as short black lines.

(C) ChIP-PCR showing percent (%) input of SUZ12 at indicated locations upstream of miR-708 in nontumorigenic breast cells (MCF10A), tumorigenic and nonmetastatic breast cancer cells (MCF7), and metastatic breast cancer cells (MDA, LM2). A 5-fold change was observed in MDA compared to MCF7. IgG was used as control. Data are representative of three independent experiments (mean ± SD).

(D) ChIP-PCR showing percent (%) input of H3K27me3 at indicated locations upstream of miR-708 in nontumorigenic breast cells (MCF10A), tumorigenic and nonmetastatic breast cancer cells (MCF7), and metastatic breast cancer cells (MDA, LM2). A 9-fold change was observed in MDA compared to MCF7. Data are representative of three independent experiments (mean ± SD).

(E) Effect of siRNA knockdown of *SUZ12* (left panel) on miR-708 expression (middle panel) and H3K27me3 (right panel) in metastatic MDA cells. Data represent mean ± SD.

See also Figure S5.

cells MCF10A and MCF7 (Figure 5C). No enrichment was detected with an isotype-matched IgG antibody. As expected from this regulated SUZ12 binding, H3K27 trimethylation in the miR-708 region was strongly enhanced in the metastatic cells, but not in the nonmetastatic cells (Figure 5D). As a control, SUZ12 target promoters *MYOD1* and *SAT2* (known targets of heterochromatin-associated H3K27me3) were efficiently pulled down with H3K27me3 antibody compared to *GAPDH* and *ACTB* (Figures S5A and S5B). These data suggest that SUZ12 interaction with the miR-708 promoter may result in the suppression of miR-708.

To further demonstrate that the PRC2 activity is directly responsible for miR-708 silencing, we performed siRNA-mediated knockdown of PRC2 subunit SUZ12. Strikingly, *SUZ12* knockdown restored expression of miR-708 in metastatic MDA breast cancer cells (Figures 5E, S5C, and S5D). Similar results were obtained with another metastatic breast cancer cell line, MDA-MB-436

(C) Initial rate of calcium regulation back to baseline. Data are represented as mean ± SEM (values for MDA control, MDA-miR-708, and MDA-miR-708-*NNAT*-mut, respectively, 0.52 ± 0.03, 0.33 ± 0.02, and 0.56 ± 0.05 with n = 115, 105, and 72 cells).

(D) Transwell cell migration assay in *NNAT* 3′ mutant UTR (MDA-miR-708-*NNAT*-mut) and miR-708 expressing MDA (MDA-miR-708) cells. Scale bars, 50 μm. Data represent the mean ± SD of six randomly selected areas from two independent experiments.

(E) Quantification of cell migration as percentage of wound healed performed with 1×10^6 MDA control, MDA-miR-708, and MDA-miR-708-*NNAT*-mut cells either in the presence of Ca^{2+} inhibitor or BAPTA-AM at 24 hr. For each cell line, cell migration is normalized to no BAPTA control. Data represent mean ± SD of nine randomly selected areas from three independent experiments.

(F) Western blots showing levels of p-ERK (T202) and p-FAK (S910) following stimulation with ATP (0 and 5 min) in MDA control, MDA-708, and MDA-miR-708-*NNAT*-mut cells. β-Actin serves as an internal control.

(G) Immunostaining of MDA control, MDA-miR-708, and MDA-miR-708-*NNAT*-mut cells for colocalization of vinculin and p-FAK in focal adhesions. Arrows indicate focal adhesions. Scale bars, 20 μm.

See also Figure S4.

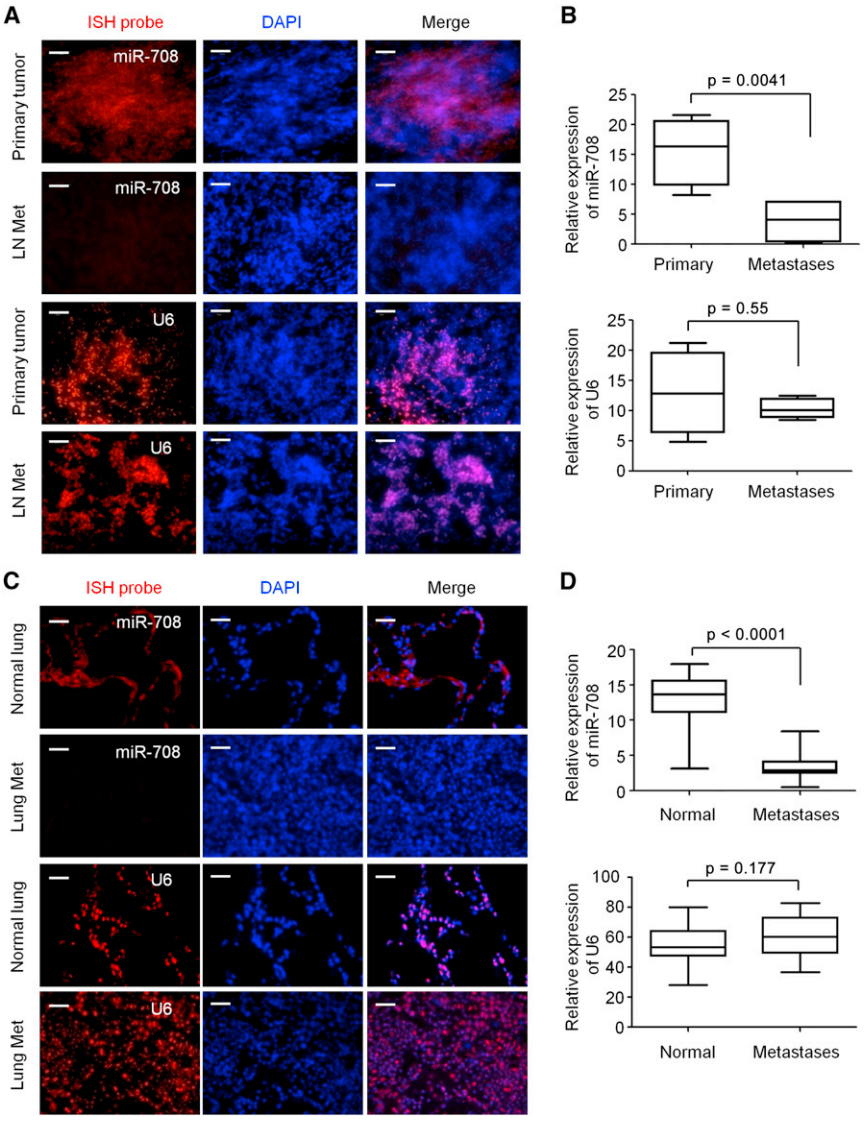

Figure 6. In Situ Hybridization Analysis Shows Reduced miR-708 Levels in Metastases of Patients with Breast Cancer

(A) Representative images showing miR-708 in situ hybridization (ISH) (red) in human primary breast tumors (Primary tumor) and matched lymph node metastases (LN Met, upper panel) and control U6 in situ hybridization (lower panel). Scale bars, 50 μm.

(B) Quantitation of miR-708 expression and control U6 expression in human primary breast tumors (Primary, n = 6) and matched lymph node metastasis (Metastases, n = 6). Data represent mean ± SD.

(C) Representative images showing miR-708 in situ hybridization (red) in lung metastases (Lung Met, upper panel) and human normal lungs (Normal lung, lower panel) and control U6 in situ hybridization. Scale bars, 50 μm.

(D) Quantitation of miR-708 expression and U6 expression in normal lungs (Normal) and lungs from patients with breast cancer with metastases (metastases, n = 10 sections each, two independent cases). Data represent mean ± SD.

See also Table S5 and Figure S6.

(Figure S5E). As expected, upregulation of miR-708 expression following *SUZ12* knockdown resulted in decreased *NNAT* expression (Figure S5F). Similarly, suppression of EZH2, another key subunit of the PRC2, also restored expression of miR-708 in metastatic MDA breast cancer cells (Figures S5G and S5H).

We next determined if the PRC2-induced H3K27 trimethylation was the cause of miR-708 suppression. Indeed, *SUZ12* knockdown resulted in decreased levels of H3K27me3 on the miR-708 upstream region (Figure 5E). These data establish that the PRC2 mediates suppression of miR-708 in metastatic breast cancer cells. To determine if the PRC2-miR-708 axis was also involved in metastasis in vivo, we examined the MMTV-PyMT breast cancer model. Evaluation of primary mammary tumors and matched lung metastases from these mice showed an inverse correlation between *Suz12* and miR-708 expression (Figures S5I, S1D, and S1E). To establish a direct connection between SUZ12 and miR-708 in the MMTV-PyMT model, we evaluated cell lines derived from MMTV-PyMT tumors (metastatic and nonmetastatic variants) (Borowsky et al., 2005). Increased miR-708 expression associated with *Nnat* suppression was observed in nonmetastatic MMTV-DB7 cells compared to the metastatic variant MMTV-Met1 (Figures S5J and S5K), consistent with observations in human breast cancer cells. As expected, siRNA-mediated knockdown of *Suz12* relieved repression of miR-708 and decreased *Nnat* levels in metastatic MMTV-Met1 cells (Figures S5L and S5M). Although there is a possibility that a repressor or a loss of a transactivator may be involved, our human and murine studies suggest that PRC2-induced H3K27 trimethylation contributes to the regulation of miR-708 expression in metastatic cancer cells.

miR-708 Expression Is Suppressed in Both Lymph Node and Distal Metastases in Patients with Breast Cancer

Next, we asked whether metastatic lesions in patients with breast cancer exhibit attenuated levels of miR-708, as observed in human breast cancer cell models and in mouse models of breast cancer that metastasizes to the lung. We analyzed a panel of frozen human primary breast tumors and matched lymph node metastases by in situ hybridization for miR-708 expression (Table S5). Strikingly, compared to primary breast tumors, miR-708 expression level was significantly reduced in matched lymph node metastases, whereas control U6 snRNA expression levels remained unchanged (Figures 6A, 6B, and S6A). We expanded this analysis by quantitated miR-708 levels in formalin-fixed paraffin-embedded (FFPE) samples using TaqMan qPCR (Table S5). Consistent with the in situ hybridization data, suppression of miR-708 was observed in metastases compared to primary

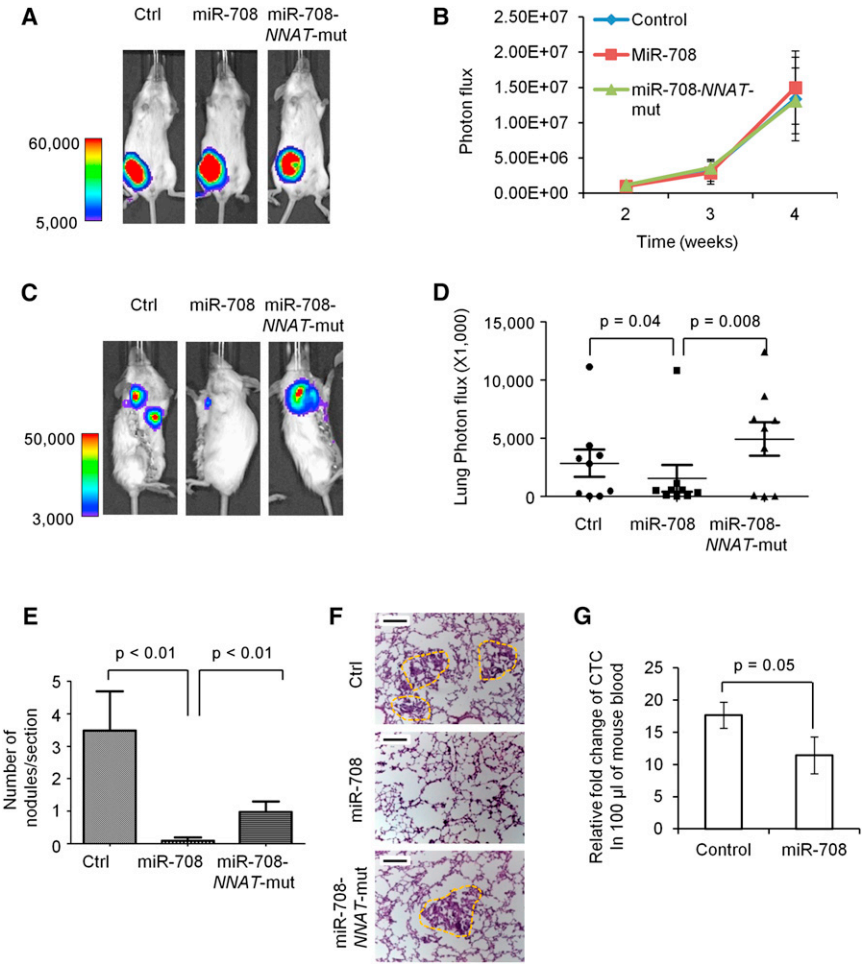

Figure 7. Neuronatin with a Mutant 3′ UTR Rescues miR-708-Mediated Metastasis Suppression In Vivo

(A) Representative bioluminescence (BLI) images of animals showing primary tumors derived from orthotopic injections of control MDA cells (Ctrl), MDA-miR-708 (miR-708) cells, and MDA-miR-708-*NNAT*-mut (miR-708-*NNAT*-mut) cells into the mammary fat pad. The color scale bar depicts the photon flux (photons per second) emitted from these mice at day 30.

(B) Quantitation of primary tumors as assessed by BLI measurements as a function of time (in weeks, n = 10 per group). Data represent mean ± SD.

(C) Representative BLI of animals from (A) showing lung metastases at day 37. Primary tumors were resected at day 30. The color scale bar depicts the photon flux (photons per second) emitted from these mice.

(D) Quantitation of pulmonary metastases as assessed by BLI measurements (day 37, n = 10 per group). Data represent mean ± SD.

(E) Number of metastatic nodules in the lungs of mice derived from primary tumors shown in (A) (ten lungs from each group, five to six sections evaluated per lung). Data represent mean ± SD.

(F) Representative H&E of lungs showing metastatic nodules. Scale bars, 50 µm.

(G) Number of CTCs in the peripheral blood of mice-bearing control LM2 (Control) cells and MDA-MB-231-LM2-miR-708 (miR-708) orthotopic tumors expressing GFP transgene. qPCR for GFP was used to determine CTC abundance in the peripheral blood. CTC numbers were determined by generating a standard curve with a predetermined number of control cells spiked into the mouse blood. Data represent mean ± SD.

See also Figure S7.

tumors (Figures S6C–S6E). Similarly, analysis of miR-708 expression in distal lung metastases in patients with breast cancer showed a dramatic reduction in miR-708 expression (Figures 6C, 6D, and S6B). We also evaluated *NNAT* expression in samples from patients with breast cancer (Table S5). As expected, *NNAT* expression inversely correlated with miR-708 expression in primary tumor and matched metastatic tissue (Figure S6F).

Having demonstrated that ectopic expression of *NNAT*-mut rescued miR-708 phenotypes pertaining to cell migration in vitro, we next determined whether *NNAT* would also rescue metastasis in vivo. We injected MDA control (or LM2 control), MDA-miR-708 (or LM2-miR-708), and MDA-miR-708-*NNAT*-mut (or LM2-miR-708-*NNAT*-mut) cells orthotopically in the mammary gland of SCID mice and allowed development of lung metastases. As expected, there was no change in primary tumor growth as determined by BLI (Figures 7A and 7B) and tumor size measurements (Figure S7). However, metastases were suppressed in MDA-miR-708, and importantly, expressing *NNAT*-mut rescued metastasis defects of MDA-miR-708 in vivo (Figures 7C and 7D). As expected, IHC analysis showed reduced number of lung metastatic nodules in LM2-miR-708 compared to controls (Figures 7E and 7F). Consistent with these observations, LM2-miR-708 tumor-bearing mice showed reduced number of circulating tumor cells (CTCs) compared to controls (Figure 7G), suggesting the possibility that miR-708-mediated inhibition of cell migration may have caused reduction in disseminated CTCs. These observations together with clinical data from patients with breast cancer showing marked suppression of miR-708 in both lymph node metastases and distal metastases compared to matched primary tumors provide a compelling rationale for developing miR-708 as a therapeutic agent against breast cancer metastasis. Given that miR-708 is a relatively unexplored miRNA, not much information is available in public databases about its expression and patient survival. Future studies are required to expand the analysis of miR-708 in metastatic lesions to a larger cohort of patients with breast cancer to determine with statistical confidence whether reduced levels of miR-708 correlate with worst patient outcome.

EXPERIMENTAL PROCEDURES

miRNA Library Construction, Deep Sequencing, and Data Analysis

Total RNA extraction, library construction, and high-throughput sequencing were performed as described (Ryu et al., 2011). Additional information is available in Supplemental Experimental Procedures.

Human Samples

Human tumor samples were collected from patients enrolled on institutional review board-approved trials at Weill Cornell Medical College and Columbia

University College of Physicians and Surgeons (New York) conducted between 1995 and 2010. Specimens were collected after obtaining written informed consent prior to undergoing any study-specific procedures in accordance with the Declaration of Helsinki. Patient's identity of pathological specimens remained anonymous in the context of this study.

Generation of miRNA and miRNA "Sponge" in Lentiviral Constructs, Virus Generation, and Transduction

To express miRNA-708 in cells, ~500 bp of pri-miRNA containing the mature miR-708 sequence 5′-AAGGAGCUUACAAUCUAGCUGGG-3′ was amplified and cloned into the pZEO lentiviral construct in fusion with a GFP reporter as described (Ryu et al., 2011). miRNA sponge was generated as described by Ebert et al. (2007). Briefly, the sponge contains 12 miR-708 binding sites, 5′-CCCAGCTAGATCATAGCTCCTT-3′, fused with GFP and driven by an *EF1α* promoter. Additional constructs and cloning methods are available in Supplemental Experimental Procedures.

Mouse Pulmonary Metastasis Models

All animal work was conducted in accordance with a protocol approved by the Institutional Animal Care and Use Committee at Weill Cornell Medical College. For orthotopic injection, 1×10^6 viable MDA control, or MDA-miR-708 cells were injected into CB-17 SCID mice fat pads in a volume of 0.1 ml. Tumor growth and pulmonary metastases (following resection of primary tumor) were monitored by live animal BLI (Xenogen IVIS system) once per week.

Intracellular Calcium Measurements

MDA control, MDA-miR-708, and MDA-miR-708-*NNAT*-mut cells were grown on coverslips for 2–3 days and then loaded with 10 μM Fura-2 (Molecular Probes), a membrane-permeable Ca^{2+}-indicator dye, at 37°C for 30 min. Cells were processed and attached to the bottom of a flowthrough superfusion chamber and mounted on the stage of an inverted epifluorescence microscope (Nikon Eclipse TE-2000). The cells in the chamber were superfused and maintained at 37°C as previously described (O'Connor and Silver, 2007). Additional information is available in Supplemental Experimental Procedures.

In Situ Hybridization with miR-708 LNA Probes

Tissue sections were obtained from primary human breast tumor and matched lymph node metastases, as well as from spontaneous primary breast tumors and matched lung metastases harvested from mice (*MMTV-PyMT;WAP-Cre; CAG-CAT-EGFP*, 15 weeks). Sections were treated and hybridized with DIG-labeled miR-708 or U6 LNA probes (Exiqon, Woburn, MA, USA) overnight at 30°C. Sections were processed further and incubated with anti-DIG Ab-POD, Fab fragments (Roche, IN, USA) overnight at 4°C.

To quantify miRNA from FFPE specimens, we isolated total RNA including small RNA using miRNeasy FFPE kit (QIAGEN) and quantified miRNA using TaqMan microRNA Assays (Applied Biosystems, CA, USA). RNU48 (Applied Biosystems) was used for normalization. Additional details are available in Supplemental Experimental Procedures.

ChIPs

ChIP assays were performed using the EZ-CHIP chromatin immunoprecipitation Kit (Millipore, CA, USA) following the manufacturer's protocol. IP complexes were immunoprecipitated with a SUZ12 antibody (Abcam; catalog #12073) and an anti-histone H3K27me3 antibody (Millipore; catalog #07-449) overnight at 4°C. Mouse IgG (negative control; Millipore, catalog #12-371B) and RNA PolII (positive control; Millipore, catalog #05-623B) were used as controls. The contents of each specific DNA locus were amplified by real-time PCR (iQ SYBR Green Supermix; Bio-Rad) using four different locations upstream of miR-708. Amplification efficiency was calculated, and the data were expressed as enrichment related to input. Additional details are available in Supplemental Experimental Procedures.

Statistical Analysis

Results are expressed as mean ± SD. Analyses of different treatment groups were performed using the nonparametric Mann-Whitney U t test using the GraphPad Prism statistical program. The p values <0.05 were considered significant. Error bars depict SD, except where indicated otherwise.

ACCESSION NUMBERS

Deep-sequencing data have been deposited in GEO with accession number GSE42313.

SUPPLEMENTAL INFORMATION

Supplemental Information includes five tables, seven figures, and Supplemental Experimental Procedures and can be found with this article online at http://dx.doi.org/10.1016/j.ccr.2012.11.019.

ACKNOWLEDGMENTS

We thank Anna Durrans and Kari Fischer for comments on the manuscript. This work was supported by funding from The Neuberger Berman Lung Cancer Laboratory, The Robert I. Goldman Foundation, and the Cornell Center on the Microenvironment and Metastasis through Award Number U54CA143876 from the NCI to V.M.

Received: September 27, 2011
Revised: September 13, 2012
Accepted: November 30, 2012
Published: January 14, 2013

REFERENCES

Ahmed, F., Wyckoff, J., Lin, E.Y., Wang, W., Wang, Y., Hennighausen, L., Miyazaki, J., Jones, J., Pollard, J.W., Condeelis, J.S., and Segall, J.E. (2002). GFP expression in the mammary gland for imaging of mammary tumor cells in transgenic mice. Cancer Res. *62*, 7166–7169.

Alvarez-Garcia, I., and Miska, E.A. (2005). MicroRNA functions in animal development and human disease. Development *132*, 4653–4662.

Asangani, I.A., Rasheed, S.A., Nikolova, D.A., Leupold, J.H., Colburn, N.H., Post, S., and Allgayer, H. (2008). MicroRNA-21 (miR-21) post-transcriptionally downregulates tumor suppressor Pdcd4 and stimulates invasion, intravasation and metastasis in colorectal cancer. Oncogene *27*, 2128–2136.

Bartel, D.P. (2004). MicroRNAs: genomics, biogenesis, mechanism, and function. Cell *116*, 281–297.

Berridge, M.J., Bootman, M.D., and Roderick, H.L. (2003). Calcium signalling: dynamics, homeostasis and remodelling. Nat. Rev. Mol. Cell Biol. *4*, 517–529.

Borowsky, A.D., Namba, R., Young, L.J., Hunter, K.W., Hodgson, J.G., Tepper, C.G., McGoldrick, E.T., Muller, W.J., Cardiff, R.D., and Gregg, J.P. (2005). Syngeneic mouse mammary carcinoma cell lines: two closely related cell lines with divergent metastatic behavior. Clin. Exp. Metastasis *22*, 47–59.

Boyer, L.A., Plath, K., Zeitlinger, J., Brambrink, T., Medeiros, L.A., Lee, T.I., Levine, S.S., Wernig, M., Tajonar, A., Ray, M.K., et al. (2006). Polycomb complexes repress developmental regulators in murine embryonic stem cells. Nature *441*, 349–353.

Bracken, C.P., Gregory, P.A., Khew-Goodall, Y., and Goodall, G.J. (2009). The role of microRNAs in metastasis and epithelial-mesenchymal transition. Cell. Mol. Life Sci. *66*, 1682–1699.

Calin, G.A., and Croce, C.M. (2006). MicroRNA signatures in human cancers. Nat. Rev. Cancer *6*, 857–866.

Calin, G.A., Sevignani, C., Dumitru, C.D., Hyslop, T., Noch, E., Yendamuri, S., Shimizu, M., Rattan, S., Bullrich, F., Negrini, M., and Croce, C.M. (2004). Human microRNA genes are frequently located at fragile sites and genomic regions involved in cancers. Proc. Natl. Acad. Sci. USA *101*, 2999–3004.

Cao, R., and Zhang, Y. (2004). SUZ12 is required for both the histone methyltransferase activity and the silencing function of the EED-EZH2 complex. Mol. Cell *15*, 57–67.

Cao, R., Wang, L., Wang, H., Xia, L., Erdjument-Bromage, H., Tempst, P., Jones, R.S., and Zhang, Y. (2002). Role of histone H3 lysine 27 methylation in Polycomb-group silencing. Science *298*, 1039–1043.

Ebert, M.S., Neilson, J.R., and Sharp, P.A. (2007). MicroRNA sponges: competitive inhibitors of small RNAs in mammalian cells. Nat. Methods *4*, 721–726.

Fidler, I.J. (2003). The pathogenesis of cancer metastasis: the 'seed and soil' hypothesis revisited. Nat. Rev. Cancer *3*, 453–458.

Gao, D., Nolan, D.J., Mellick, A.S., Bambino, K., McDonnell, K., and Mittal, V. (2008). Endothelial progenitor cells control the angiogenic switch in mouse lung metastasis. Science *319*, 195–198.

Gregory, P.A., Bert, A.G., Paterson, E.L., Barry, S.C., Tsykin, A., Farshid, G., Vadas, M.A., Khew-Goodall, Y., and Goodall, G.J. (2008). The miR-200 family and miR-205 regulate epithelial to mesenchymal transition by targeting ZEB1 and SIP1. Nat. Cell Biol. *10*, 593–601.

Gupta, G.P., and Massagué, J. (2006). Cancer metastasis: building a framework. Cell *127*, 679–695.

Guy, C.T., Cardiff, R.D., and Muller, W.J. (1992). Induction of mammary tumors by expression of polyomavirus middle T oncogene: a transgenic mouse model for metastatic disease. Mol. Cell. Biol. *12*, 954–961.

Hoth, M., and Penner, R. (1992). Depletion of intracellular calcium stores activates a calcium current in mast cells. Nature *355*, 353–356.

Huang, C., Jacobson, K., and Schaller, M.D. (2004). MAP kinases and cell migration. J. Cell Sci. *117*, 4619–4628.

Huang, Q., Gumireddy, K., Schrier, M., le Sage, C., Nagel, R., Nair, S., Egan, D.A., Li, A., Huang, G., Klein-Szanto, A.J., et al. (2008). The microRNAs miR-373 and miR-520c promote tumour invasion and metastasis. Nat. Cell Biol. *10*, 202–210.

Hunger-Glaser, I., Fan, R.S., Perez-Salazar, E., and Rozengurt, E. (2004). PDGF and FGF induce focal adhesion kinase (FAK) phosphorylation at Ser-910: dissociation from Tyr-397 phosphorylation and requirement for ERK activation. J. Cell. Physiol. *200*, 213–222.

Ilić, D., Furuta, Y., Kanazawa, S., Takeda, N., Sobue, K., Nakatsuji, N., Nomura, S., Fujimoto, J., Okada, M., and Yamamoto, T. (1995). Reduced cell motility and enhanced focal adhesion contact formation in cells from FAK-deficient mice. Nature *377*, 539–544.

Inui, M., Martello, G., and Piccolo, S. (2010). MicroRNA control of signal transduction. Nat. Rev. Mol. Cell Biol. *11*, 252–263.

Iorio, M.V., Ferracin, M., Liu, C.G., Veronese, A., Spizzo, R., Sabbioni, S., Magri, E., Pedriali, M., Fabbri, M., Campiglio, M., et al. (2005). MicroRNA gene expression deregulation in human breast cancer. Cancer Res. *65*, 7065–7070.

Joseph, R., Dou, D., and Tsang, W. (1994). Molecular cloning of a novel mRNA (neuronatin) that is highly expressed in neonatal mammalian brain. Biochem. Biophys. Res. Commun. *201*, 1227–1234.

Joyce, J.A., and Pollard, J.W. (2009). Microenvironmental regulation of metastasis. Nat. Rev. Cancer *9*, 239–252.

Kang, S.Y., Halvorsen, O.J., Gravdal, K., Bhattacharya, N., Lee, J.M., Liu, N.W., Johnston, B.T., Johnston, A.B., Haukaas, S.A., Aamodt, K., et al. (2009). Prosaposin inhibits tumor metastasis via paracrine and endocrine stimulation of stromal p53 and Tsp-1. Proc. Natl. Acad. Sci. USA *106*, 12115–12120.

Kleer, C.G., Cao, Q., Varambally, S., Shen, R., Ota, I., Tomlins, S.A., Ghosh, D., Sewalt, R.G., Otte, A.P., Hayes, D.F., et al. (2003). EZH2 is a marker of aggressive breast cancer and promotes neoplastic transformation of breast epithelial cells. Proc. Natl. Acad. Sci. USA *100*, 11606–11611.

Koyanagi, M., Baguet, A., Martens, J., Margueron, R., Jenuwein, T., and Bix, M. (2005). EZH2 and histone 3 trimethyl lysine 27 associated with Il4 and Il13 gene silencing in Th1 cells. J. Biol. Chem. *280*, 31470–31477.

Lin, H.H., Bell, E., Uwanogho, D., Perfect, L.W., Noristani, H., Bates, T.J., Snetkov, V., Price, J., and Sun, Y.M. (2010). Neuronatin promotes neural lineage in ESCs via Ca(2+) signaling. Stem Cells *28*, 1950–1960.

Lu, J., Getz, G., Miska, E.A., Alvarez-Saavedra, E., Lamb, J., Peck, D., Sweet-Cordero, A., Ebert, B.L., Mak, R.H., Ferrando, A.A., et al. (2005). MicroRNA expression profiles classify human cancers. Nature *435*, 834–838.

Lujambio, A., Calin, G.A., Villanueva, A., Ropero, S., Sánchez-Céspedes, M., Blanco, D., Montuenga, L.M., Rossi, S., Nicoloso, M.S., Faller, W.J., et al. (2008). A microRNA DNA methylation signature for human cancer metastasis. Proc. Natl. Acad. Sci. USA *105*, 13556–13561.

Ma, L., Teruya-Feldstein, J., and Weinberg, R.A. (2007). Tumour invasion and metastasis initiated by microRNA-10b in breast cancer. Nature *449*, 682–688.

Magalhaes, G.S., Muotri, A.R., Marchetto, M.C., Menck, C.F., and Ventura, A.M. (2002). An adenovirus vector containing the suicide gene thymidine kinase for a broad application in cancer gene therapy. Mem. Inst. Oswaldo Cruz *97*, 547–552.

Margueron, R., Justin, N., Ohno, K., Sharpe, M.L., Son, J., Drury, W.J., 3rd, Voigt, P., Martin, S.R., Taylor, W.R., De Marco, V., et al. (2009). Role of the polycomb protein EED in the propagation of repressive histone marks. Nature *461*, 762–767.

Marson, A., Levine, S.S., Cole, M.F., Frampton, G.M., Brambrink, T., Johnstone, S., Guenther, M.G., Johnston, W.K., Wernig, M., Newman, J., et al. (2008). Connecting microRNA genes to the core transcriptional regulatory circuitry of embryonic stem cells. Cell *134*, 521–533.

Minn, A.J., Gupta, G.P., Siegel, P.M., Bos, P.D., Shu, W., Giri, D.D., Viale, A., Olshen, A.B., Gerald, W.L., and Massagué, J. (2005). Genes that mediate breast cancer metastasis to lung. Nature *436*, 518–524.

Nolan, D.J., Ciarrocchi, A., Mellick, A.S., Jaggi, J.S., Bambino, K., Gupta, S., Heikamp, E., McDevitt, M.R., Scheinberg, D.A., Benezra, R., and Mittal, V. (2007). Bone marrow-derived endothelial progenitor cells are a major determinant of nascent tumor neovascularization. Genes Dev. *21*, 1546–1558.

O'Connor, N., and Silver, R.B. (2007). Ratio imaging: practical considerations for measuring intracellular Ca2+ and pH in living cells. Methods Cell Biol. *81*, 415–433.

Ozen, M., Creighton, C.J., Ozdemir, M., and Ittmann, M. (2008). Widespread deregulation of microRNA expression in human prostate cancer. Oncogene *27*, 1788–1793.

Pettit, E.J., and Fay, F.S. (1998). Cytosolic free calcium and the cytoskeleton in the control of leukocyte chemotaxis. Physiol. Rev. *78*, 949–967.

Ryu, S., Joshi, N., McDonnell, K., Woo, J., Choi, H., Gao, D., McCombie, W.R., and Mittal, V. (2011). Discovery of novel human breast cancer microRNAs from deep sequencing data by analysis of pri-microRNA secondary structures. PLoS One *6*, e16403.

Saini, S., Majid, S., Shahryari, V., Arora, S., Yamamura, S., Chang, I., Zaman, M.S., Deng, G., Tanaka, Y., and Dahiya, R. (2012). miRNA-708 control of CD44(+) prostate cancer-initiating cells. Cancer Res. *72*, 3618–3630.

Schwartz, Y.B., and Pirrotta, V. (2007). Polycomb silencing mechanisms and the management of genomic programmes. Nat. Rev. Genet. *8*, 9–22.

Sellers, W.R., and Loda, M. (2002). The EZH2 polycomb transcriptional repressor—a marker or mover of metastatic prostate cancer? Cancer Cell *2*, 349–350.

Shimono, Y., Zabala, M., Cho, R.W., Lobo, N., Dalerba, P., Qian, D., Diehn, M., Liu, H., Panula, S.P., Chiao, E., et al. (2009). Downregulation of miRNA-200c links breast cancer stem cells with normal stem cells. Cell *138*, 592–603.

Sieg, D.J., Hauck, C.R., and Schlaepfer, D.D. (1999). Required role of focal adhesion kinase (FAK) for integrin-stimulated cell migration. J. Cell Sci. *112*, 2677–2691.

Simon, J.A., and Kingston, R.E. (2009). Mechanisms of polycomb gene silencing: knowns and unknowns. Nat. Rev. Mol. Cell Biol. *10*, 697–708.

Steeg, P.S. (2006). Tumor metastasis: mechanistic insights and clinical challenges. Nat. Med. *12*, 895–904.

Stegmeier, F., Hu, G., Rickles, R.J., Hannon, G.J., and Elledge, S.J. (2005). A lentiviral microRNA-based system for single-copy polymerase II-regulated RNA interference in mammalian cells. Proc. Natl. Acad. Sci. USA *102*, 13212–13217.

Suh, Y.H., Kim, W.H., Moon, C., Hong, Y.H., Eun, S.Y., Lim, J.H., Choi, J.S., Song, J., and Jung, M.H. (2005). Ectopic expression of Neuronatin potentiates adipogenesis through enhanced phosphorylation of cAMP-response element-binding protein in 3T3-L1 cells. Biochem. Biophys. Res. Commun. *337*, 481–489.

Suzuki, H., Takatsuka, S., Akashi, H., Yamamoto, E., Nojima, M., Maruyama, R., Kai, M., Yamano, H.O., Sasaki, Y., Tokino, T., et al. (2011). Genome-wide

profiling of chromatin signatures reveals epigenetic regulation of MicroRNA genes in colorectal cancer. Cancer Res. *71*, 5646–5658.

Swanson, K.D., Reigh, C., and Landreth, G.E. (1998). ATP-stimulated activation of the mitogen-activated protein kinases through ionotrophic P2X2 purinoreceptors in PC12 cells. Difference in purinoreceptor sensitivity in two PC12 cell lines. J. Biol. Chem. *273*, 19965–19971.

Tavazoie, S.F., Alarcón, C., Oskarsson, T., Padua, D., Wang, Q., Bos, P.D., Gerald, W.L., and Massagué, J. (2008). Endogenous human microRNAs that suppress breast cancer metastasis. Nature *451*, 147–152.

Valastyan, S., and Weinberg, R.A. (2009). MicroRNAs: crucial multi-tasking components in the complex circuitry of tumor metastasis. Cell Cycle *8*, 3506–3512.

Valastyan, S., Reinhardt, F., Benaich, N., Calogrias, D., Szász, A.M., Wang, Z.C., Brock, J.E., Richardson, A.L., and Weinberg, R.A. (2009). A pleiotropically acting microRNA, miR-31, inhibits breast cancer metastasis. Cell *137*, 1032–1046.

Vandewalle, B., Hornez, L., Revillion, F., and Lefebvre, J. (1994). Effect of extracellular ATP on breast tumor cell growth, implication of intracellular calcium. Cancer Lett. *85*, 47–54.

Ventura, A., Young, A.G., Winslow, M.M., Lintault, L., Meissner, A., Erkeland, S.J., Newman, J., Bronson, R.T., Crowley, D., Stone, J.R., et al. (2008). Targeted deletion reveals essential and overlapping functions of the miR-17 through 92 family of miRNA clusters. Cell *132*, 875–886.

Volinia, S., Calin, G.A., Liu, C.G., Ambs, S., Cimmino, A., Petrocca, F., Visone, R., Iorio, M., Roldo, C., Ferracin, M., et al. (2006). A microRNA expression signature of human solid tumors defines cancer gene targets. Proc. Natl. Acad. Sci. USA *103*, 2257–2261.

Yang, S., Zhang, J.J., and Huang, X.Y. (2009). Orai1 and STIM1 are critical for breast tumor cell migration and metastasis. Cancer Cell *15*, 124–134.

Zhao, J., and Guan, J.L. (2009). Signal transduction by focal adhesion kinase in cancer. Cancer Metastasis Rev. *28*, 35–49.

Zheng, Y., Xia, Y., Hawke, D., Halle, M., Tremblay, M.L., Gao, X., Zhou, X.Z., Aldape, K., Cobb, M.H., Xie, K., et al. (2009). FAK phosphorylation by ERK primes ras-induced tyrosine dephosphorylation of FAK mediated by PIN1 and PTP-PEST. Mol. Cell *35*, 11–25.

Zhu, S., Wu, H., Wu, F., Nie, D., Sheng, S., and Mo, Y.Y. (2008). MicroRNA-21 targets tumor suppressor genes in invasion and metastasis. Cell Res. *18*, 350–359.